Journal of Marine Research, 45, 83–105, 1987

Solutions for internal tidal generation over coastal topography

by P. D. Craig[1,2]

ABSTRACT

Internal tides may be described by a hyperbolic equation which, for the case of constant buoyancy frequency, has constant coefficients. The equation is solved by using the characteristic geometry and characteristic functions to establish a set of linear algebraic equations in the modal amplitudes. The accuracy of the solutions can be assessed using energy considerations. The capability of the solution technique is demonstrated by simulating the barotropic generation of internal waves over linear topography, with emphasis on near-critical topography, when the solution exhibits high shears and discontinuous behavior at the critical slope. The structure of the waves is determined by the ratio, α, of the bottom slope to characteristic slope. The magnitude of the waves may be estimated by considering the ratio of the baroclinic to the topographic length scales which, for linear slopes, is also given by α. For supercritical slopes, the offshore energy flux varies approximately linearly with α, while for subcritical slopes it varies as α^5.

1. Introduction

Internal tides are often a dominant feature of the water motion over continental slope topography. Here, the movement due to the barotropic tides distorts the equilibrium density field up or down the slope, causing a baroclinic pressure gradient and a resultant secondary motion at the tidal frequency.

Theoretical models of internal tides have largely been developed on the assumption of two-dimensional, linear, inviscid dynamics. Rattray (1960) pioneered the theoretical description with a model of a two-layered ocean over stepped topography. The model was extended to include continuous stratification by Rattray *et al.* (1969) and Prinsenberg *et al.* (1974).

With the introduction of continuous stratification, the dynamics may be described by a single linear, second-order hyperbolic equation, which will be discussed in Section 2 of the present paper. If the buoyancy frequency is constant, the equation may be integrated analytically along the characteristics. However, despite the simplicity of the integration, solution techniques tend to be complicated by the boundary conditions,

1. CSIRO Division of Oceanography, GPO Box 1538, Hobart, Tasmania 7001, Australia.
2. Previous address: University of Western Australia, Nedlands, Western Australia, 6009.

which include the requirement for a radiation condition on at least one lateral boundary.

Two solution techniques applicable to finite width topography utilize the properties of the characteristics. The first, developed by Sandstrom (1976), introduces a transformation of the horizontal coordinate in such a way that successive surface reflections of a characteristic occur unit distance apart. This enables the solution to be represented as a Fourier series in the horizontal coordinate. The second, developed by Baines (1973; 1974; 1982), expresses the lateral boundary condition as a Cauchy-principal-valued integral, leading to a restatement of the problem as a Fredholm integral equation.

The relationship between the stratification and the topography is specified by the parameter denoted in the present paper as α, defined as the ratio of the bottom slope to the characteristic slope. Values of α less than, equal to and greater than one define subcritical, critical and supercritical bottom slopes respectively. An increase in α from a value less than one to greater than one, caused by an increasing stratification, can lead to a dramatic change in the two-dimensional characteristic geometry, and a corresponding dramatic modification of the internal tidal solutions.

The solution procedures of Sandstrom (1976) and Baines (1982) both require considerable modification of the formalism if segments of the topography are supercritical.

An alternative technique that is equally applicable to subcritical and supercritical topography will be introduced in Section 3 of the present paper. This technique uses geometric considerations, based on the characteristic configuration, to reduce the internal wave problem to a set of linear algebraic equations, the equation unknowns being the amplitudes of the internal modes. The accuracy of the solutions so derived depends on the number of modal amplitudes determined, and may be assessed using energy conservation.

The technique will be applied, in Section 4, to the generation of internal tides over a linear slope. The emphasis of the solutions described will be on the behavior at near-critical slopes, and the change in dynamics with the transition through critical. Presentation of the solution stream function enables the two-dimensional structure of the waves to be visualized, and highlights the close relationship between the geometry of the characteristics and the internal waves.

Aspects of the internal wave generation can be clarified using scaling analysis, which will be discussed in Section 5. The energy of the internal tides is dependent on the ratio of the baroclinic length scale to the topographic length scale which, for linear slopes, is again given by α. The offshore energy flux varies approximately as α^5 for $\alpha < 1$, but varies linearly for $\alpha > 1$. The onshore energy flux varies as α^5 for all α, but is discontinuous at $\alpha = 1$, decreasing, in the example considered, by two orders of magnitude with the transition through $\alpha = 1$.

For near-critical topography, there is a narrow band of highly sheared, energetic

motion. This band is directed upslope and onshore for α subcritical, but downslope and offshore for α supercritical. In reality, the motion in these bands will be strongly modified by frictional and nonlinear effects not included in the model.

2. Equations of motion

We consider an incompressible, inviscid, stably stratified fluid, with equilibrium density given by $\rho_0(z)$. Coordinates are Cartesian, with x crossshore, y longshore and z vertical. The motion is assumed to be hydrostatic, with no longshore variation and of small enough amplitude that it may be described by linear equations. If p and ρ are the pressure and density perturbations away from the rest state, and u, v and w are the x, y and z velocity components respectively, then the appropriate equations are (e.g. Wunsch, 1968):

$$\rho_0(u_t - fv) = -p_x, \tag{2.1}$$

$$\rho_0(v_t + fu) = 0, \tag{2.2}$$

$$0 = -p_z - \rho g, \tag{2.3}$$

$$\rho_t + w\rho_{0z} = 0, \tag{2.4}$$

$$u_x + w_z = 0, \tag{2.5}$$

where t represents time, f is the Coriolis parameter, and alphabetic subscripts represent differentiation.

The Boussinesq approximation is assumed valid so that, in (2.1) and (2.2), ρ_0 may be considered constant while its vertical derivative, ρ_{0z} in (2.4), may be regarded as nonzero (e.g. Wunsch, 1968; 1969). The buoyancy frequency N, defined by

$$N^2 = -\frac{g}{\rho_0}\rho_{0z}, \tag{2.6}$$

will be taken as constant.

The time dependence of the variables in (2.1) to (2.5) may be assumed to be of the form $\exp(-i\omega t)$, for real positive frequency ω. The hydrostatic approximation in (2.3) is equivalent to the assumption that $\omega^2 \ll N^2$.

By (2.5), a stream function ψ may be defined by

$$u = -\psi_z e^{-i\omega t}, \qquad w = \psi_x e^{-i\omega t}. \tag{2.7}$$

Equations (2.1) to (2.4) can be reduced to a single equation in ψ given by

$$\psi_{xx} - c^2\psi_{zz} = 0, \tag{2.8}$$

where

$$c = (\omega^2 - f^2)^{1/2}/N. \tag{2.9}$$

Equation (2.8) is hyperbolic, and may be rewritten

$$\psi_{\xi\eta} = 0, \tag{2.10}$$

where

$$\xi = z + cx \qquad \text{and} \qquad \eta = z - cx \tag{2.11}$$

are the characteristic coordinates. Now,

$$\psi(\xi, \eta) = \phi(\xi) + \gamma(\eta), \tag{2.12}$$

where ϕ and γ are described as 'the characteristic functions'. The pressure is given, to within an arbitrary constant, by

$$p = i\rho_0 N \frac{(\omega^2 - f^2)^{1/2}}{\omega} (-\phi(\xi) + \gamma(\eta))e^{-i\omega t}. \tag{2.13}$$

The solution domain has the form shown in Figure 1, representative of coastal ocean geometry. The mean position of the free surface is $z = H$, a constant, and the lower boundary is $z = h(x)$, with the slope $h_x(x)$ assumed non-negative. Variations in the topography are assumed to be of limited extent, so that $h(x) = 0$ for $x < x_1$, representing the deep ocean, and $h(x) = h_0$, a positive constant, for $x > x_2$, representing the continental shelf. The domain boundary $x = 0$ is assumed open, and the coastline is given by $x = L$.

The bottom boundary condition for ψ is

$$\psi = 0 \qquad \text{on} \qquad z = h(x). \tag{2.14}$$

At the free surface, $z = H$, the linear boundary conditions are

$$p = \rho_0 g\zeta \qquad \text{and} \qquad w = -i\omega\zeta, \tag{2.15}$$

(e.g. Gill, 1982) where ζ is the free surface displacement. In terms of ψ,

$$\psi_z = -\frac{g}{\omega^2}\psi_{xx} \qquad \text{on} \qquad z = H. \tag{2.16}$$

The slope-ratio parameter α, introduced in Section 1, is defined by

$$\alpha = \frac{h_x}{c}. \tag{2.17}$$

For general topography, α will be a function of x. The significance of α will become apparent in following sections.

In constant-depth water, the solution to (2.8) satisfying (2.14) and (2.16) may be obtained by separation of variables to give the familiar decomposition into orthogonal modes (e.g. LeBlond and Mysak, 1978; Gill 1982). At length scales relevant to the

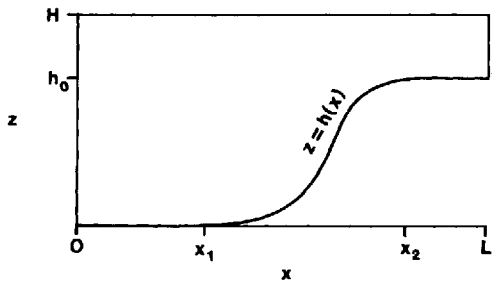

Figure 1. The solution domain, representing continental shelf and slope bathymetry.

coastal ocean, the barotropic mode is given, for $x < x_1$, by

$$\psi = z \exp(ick_0 x), \tag{2.18}$$

where

$$k_0 = \pm\left(\frac{N^2}{gH}\right)^{1/2}, \tag{2.19}$$

and the baroclinic modes by

$$\psi = \sin k_n z \exp(ick_n x), \tag{2.20}$$

where

$$k_n = \frac{n\pi}{H}, \qquad n = \pm 1, \pm 2, \ldots \tag{2.21}$$

At this order of approximation, there is no (depth-integrated) horizontal mass flux or surface displacement associated with the internal modes.

A stream function solution of the form (2.18) or (2.20), with $\exp(-i\omega t)$ time-dependence, represents a wave with energy propagation in the positive x-direction if k is positive, and in the negative x-direction if k is negative. The phase propagation is, in each case, in the same direction. The radiation condition requires that, at open boundaries, the solution must be expressed as a sum of modes, each of which has the required direction of energy propagation (e.g. Baines, 1973).

In the present study, we wish to examine the generation of baroclinic modes by a barotropic wave, representing the surface tide, incident on coastal topography of the type shown in Figure 1. The form of the barotropic wave may be simplified because the topographic length scale L, of the order of hundreds of kilometers, is much less than the barotropic wavelength, $2\pi/k_0 c$, of the order of thousands of kilometers. As a result of this contrast in length scales, the surface condition (2.16) may be approximated by

$$\psi_{xx} = 0 \qquad \text{on} \qquad z = H. \tag{2.22}$$

In the case of strictly barotropic motion, when $N \equiv 0$, the solution to (2.8), satisfying (2.14) and (2.22), is

$$\psi = -i\omega\zeta_0(x - L)\,\frac{z - h}{H - h}, \tag{2.23}$$

where ζ_0 is the barotropic surface tidal amplitude at the coast.

The solution (2.23) was derived by Battisti and Clarke (1982) as a model of the barotropic M_2 tide. Their model also includes a wavelike dependence on the longshore coordinate, which has been ignored in the present formulation.

In the presence of stratification, when N is nonzero, the barotropic mode will continue to be given by (2.23) over the flat sections of the topography, $x < x_1$ and $x > x_2$. That is, over the flat topography, the amplitude of the barotropic mode is unaffected by the presence of stratification. This result follows necessarily because the barotropic mode accounts for all the surface displacement and depth-integrated transport.

We are now in a position to state fully the problem to be solved. We seek a solution to (2.8), satisfying the bottom condition (2.14) and the surface condition (2.22). For $x < x_1$, the solution is required to have the form

$$\psi = -\frac{i\omega\zeta_0 z}{H}(x - L) + 2i\sum_{n\geq 1} a_n e^{-ick_n x}\sin k_n z, \tag{2.24}$$

where ζ_0 is specified, and the a_n, $n = 1, 2, \ldots$, are the (unknown) amplitudes of the reflected waves. For $x > x_2$,

$$\psi = -\frac{i\omega\zeta_0(z - h_0)}{H - h_0}(x - L) + 2i\sum_{n\geq 0} b_n e^{ick_n x}\sin \ell_n(z - h_0), \tag{2.25}$$

where

$$\ell_n = n\pi/(H - h_0),\ n = 1, 2, \ldots, \tag{2.26}$$

and the b_n, $n = 1, 2, \ldots$, are the (unknown) amplitudes of the transmitted waves. The factor $2i$ is included in (2.24) and (2.25) for later convenience.

In (2.25), the coastal boundary is assumed reflective to the barotropic mode but transmissive to the baroclinic modes. The boundary will exert a strong influence on the barotropic wave because the shelf width is so much less than the wavelength. By contrast, the shelf width is usually considerably longer than the first-mode baroclinic wavelength so that internal waves of tidal frequency are effectively damped before being reflected by the coastal wall (e.g. Prinsenberg *et al.*, 1974; Baines, 1982).

3. Solution technique

The earliest solutions to the problem defined at the end of the previous section were determined for the special topographies of a step (Rattray *et al.*, 1969, and Prinsen-

berg *et al.*, 1974) and a strictly supercritical slope (Prinsenberg and Rattray, 1975). In these cases, the solution representation (2.24) holds for $x < x_1$, where x_1 is assumed to be the location of the step or shelf break. The amplitudes a_n and b_n can then be determined by requiring continuity of ψ and ψ_x at $x = x_1$ for $z > h_0$, with $\psi = 0$ on the slope face.

For arbitrarily complicated topography, the solution for ψ may be determined by a technique that may be regarded as a conceptual extension of this matching procedure. Now the modal representations (2.24) and (2.25) cannot be equated at the same point in space, but must be matched across the domain using the characteristic functions.

The characteristic functions for $x < x_1$ are determined from (2.24). At $x = 0$, where $\zeta = \eta = z$, ϕ and γ may be expressed as functions of z,

$$\phi_1(z) = -\frac{i\omega\zeta_0}{2H}\left(\frac{z^2}{2c} - Lz\right) - \sum_{n\geq 1} a_n \exp(-ik_n z) - a_0, \tag{3.1}$$

and

$$\gamma_1(z) = \frac{i\omega\zeta_0}{2H}\left(\frac{z^2}{2c} + Lz\right) + \sum_{n\geq 1} a_n \exp(ik_n z) + a_0, \tag{3.2}$$

where the subscripts 1 have been introduced to indicate evaluation at $x = 0$.

Inclusion of the constant a_0 gives the most general form of ϕ and γ. However, it does not affect the solution for ψ and does not enter the surface or bottom boundary conditions. Thus, a_0 may be arbitrarily set to zero. At $x = L$, $\xi = z + cL$, $\eta = z - cL$ and ϕ and γ may again be expressed as functions of z,

$$\phi_2(z) = -\frac{i\omega\zeta_0(z - h_0)^2}{4c(H - h_0)} + \sum_{n\geq 0} b_n \exp(i\ell_n(z - h_0 + cL)), \tag{3.3}$$

and

$$\gamma_2(z) = \frac{i\omega\zeta_0(z - h_0)^2}{4c(H - h_0)} - \sum_{n\geq 0} b_n \exp(-i\ell_n(z - h_0 - cL)), \tag{3.4}$$

where subscript 2 indicates evaluation at $x = L$. It is essential to retain the constant b_0 in these expressions for ϕ and γ. Once a_0 has been set, the constant b_0 is no longer arbitrary. It will have no effect on the solution for ψ, but will appear in the expression for the pressure. Without the inclusion of b_0, energy conservation cannot be satisfied and the solution procedure will not converge.

The function ϕ is constant along characteristics of negative slope (ξ = constant), while γ is constant along characteristics of positive slope (η = constant). For any characteristic ξ = constant, intersecting the boundary $z = h(x)$ or $z = H$, we may consider the reflected characteristic η = constant, as shown in Figure 2. At the point of intersection with the bottom boundary

$$\phi = -\gamma, \tag{3.5}$$

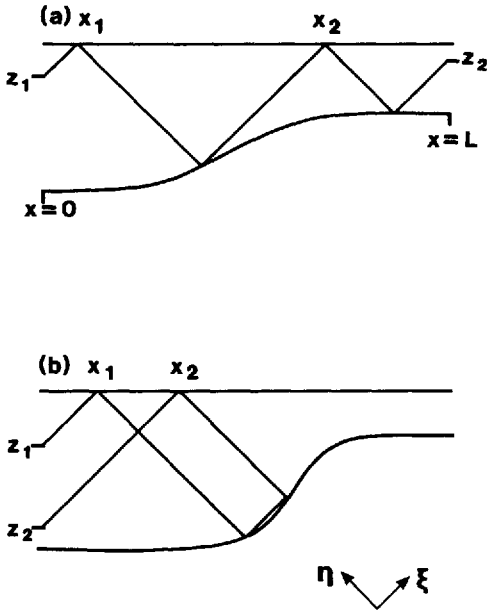

Figure 2. Successive characteristic reflections in a domain with (a) strictly subcritical bottom topography and (b) a supercritical bottom segment. z_1 and z_2 are the z-coordinates of the initial and final points of the characteristic trace, and x_1 and x_2 are x-coordinates of the surface reflections.

by (2.14), while at the point of intersection with the surface, by (2.22) and (2.23),

$$\phi + \gamma = -i\omega\zeta_0(x_R - L), \tag{3.6}$$

where x_R is the x-coordinate of the surface intersection. It is thus possible to trace the characteristic, and the appropriate characteristic function values, through the domain, as shown in Figure 2. In Figure 2a, the bottom slope is everywhere subcritical (i.e. $\alpha < 1$), and the characteristic from $x = 0$ terminates at $x = L$. If the bottom slope is supercritical (i.e. $\alpha > 1$) in places, a characteristic originating at $x = 0$ may be reflected back to $x = 0$. This situation is shown in Figure 2b.

For every characteristic trace we obtain a relationship between characteristic function values at $x = 0$ and either at $x = L$ (Fig. 2a) or $x = 0$ (Fig. 2b). The characteristic path in Figure 2a, for example, would lead to the equation

$$\gamma_2(z_2) = \gamma_1(z_1) + i\omega\zeta_0(x_1 + x_2 - 2L), \tag{3.7}$$

while the path in Figure 2b would give

$$\gamma_1(z_2) = \gamma_1(z_1) + i\omega\zeta_0(x_1 - x_2), \tag{3.8}$$

where z_1 and z_2 are the z-values at the end points, and x_1 and x_2 are the x-coordinates of

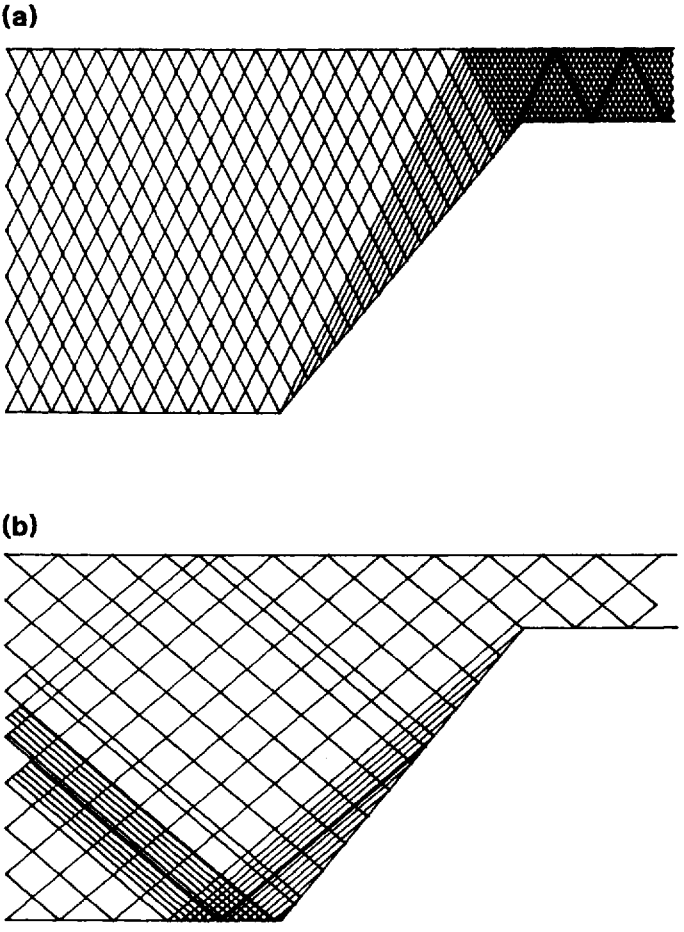

Figure 3. Two examples of characteristic traces for (a) $\alpha = .6$ and (b) $\alpha = 1.4$. The traces are generated in each case by 16 characteristics originating at 9 equally spaced points on $x = 0$.

the surface reflections, as shown in Figure 2. The relationship between the characteristic functions, exemplified by (3.7) and (3.8), is in fact a linear algebraic equation in the modal coefficients a_n and b_n.

If the solution at $x = 0$ is to be represented by K modes (that is, the series in (3.1) and (3.2) are to be truncated at the Kth term), then K separate characteristic traces must be undertaken. This may be achieved as follows. The total depth at $x = 0$ is divided into $K/2$ subintervals of size $\Delta z = 2H/K$. The positive slope characteristic is traced from $z = 0$, both characteristics from $z = \Delta z, 2\Delta z, \ldots (K/2 - 1)\Delta z$, and finally, the negative slope characteristic from $z = H$. Two examples of this tracing procedure are shown in Figure 3, one for subcritical bottom topography, and the second for supercritical. For these examples, $K = 16$.

At this stage, K (z_1, z_2) pairs are established. If M is the number of coefficients b_n to be evaluated then, accounting for the constant b_0, $M - 1$ modes can be represented at $x = L$. A further M characteristic traces are then undertaken by dividing the z-interval (h_0, H) at $x = L$ into $M/2$ segments, and following characteristics from each of the nodes, as was done from $x = 0$. The traces establish a further M (z_1, z_2) pairs.

All the information about the bottom shape that is required for the solution is contained in the $K + M$ (z_1, z_2) pairs. In this sense, the $K + M$ pairs represent a projection of the bottom geometry by the characteristics onto the lines $x = 0$ and $x = L$. In some ways, the pairs represent a discretization of the 'phase function' used by Sandstrom (1976), which was essentially a description of the projection of the bottom geometry by the characteristics onto the line $z = H$.

Using equations of the form (3.7) and (3.8), it is now possible to set up $K + M$ linear equations in $a_1, a_2, \ldots a_K, b_0, \ldots b_{M-1}$. A single matrix inversion is then required to determine the solution. It should be noted that the $K + M$ equations are complex, so that the coefficient matrix will be complex with dimension $(K + M) \times (K + M)$.

The $K + M$ linear equations express the relationship between the characteristic functions at $x = 0$ and $x = L$. The equations may thus be considered as a discrete equivalent of Baines's (1973) Fredholm integral equation, which expressed the relationship between the characteristic functions in analytic form.

Once the coefficients a_n and b_n are determined, the solution for ψ is determined, at least to within the approximation implied by the modal series truncation, at $x = 0$ and $x = L$. The values of ψ can be calculated at internal points simply as the sum of the characteristic functions.

The technique will, of course, give an accurate representation of the solution only if the first K modes for $x < x_1$ and the first M modes for $x > x_2$ carry most of the energy of the flow. Assuming the modal representations (2.24) and (2.25) converge, then K and M can be made large enough for the energy of the truncated modal series to fall within specified limits of the energy of the infinite series.

The convergence of a solution may be assessed using energy flux calculations. Since there are no energy sources in the solution domain, the total, time-averaged energy flux through the domain boundary should be zero.

The energy flux through a vertical section is given by

$$F = \int_{\text{depth}} \frac{1}{4}(p^*u + u^*p)dz, \tag{3.9}$$

(e.g. LeBlond and Mysak, 1978) where * denotes the complex conjugate, and u and p may be calculated from (2.7) and (2.13). Thus the energy flux due strictly to the reflected baroclinic modes is

$$F_1 = \rho_0 N \frac{(\omega^2 - f^2)^{1/2}}{\omega} \pi \sum_{n \geq 1} n\, a_n a_n^*, \tag{3.10}$$

on $x < x_1$, while that due to the transmitted baroclinic waves on $x > x_2$ is

$$F_2 = \rho_0 N \frac{(\omega^2 - f^2)^{1/2}}{\omega} \pi \sum_{n \geq 1} n\, b_n b_n^*. \tag{3.11}$$

The total flux for $x < x_1$ and $x > x_2$ also involves a contribution from the barotropic pressure multiplied by the baroclinic velocity component. While these cross-terms must be included in the energy balance calculation, they actually average out to zero over a full first-mode baroclinic wavelength. Thus, F_1 and F_2 may be regarded as the baroclinic fluxes for $x < x_1$ and $x > x_2$. Strictly, they are the depth-integrated, horizontally- and time-averaged baroclinic energy fluxes on $x < x_1$ and $x > x_2$ respectively.

There is no energy flux through $z = h(x)$, but at $z = H$, the surface, there is a nonzero flux resulting from the vertical barotropic velocity and the baroclinic pressure. While the fluxes at $x = 0$ and $x = L$ can be integrated analytically, that through $z = H$ must be numerically integrated. By tracing characteristics from $z = H$ back to $x = 0$, the baroclinic pressure can be determined at any point on $z = H$, so that the numerical integration can be performed accurately. The flux calculations are straightforward and will not be described in further detail.

For the solutions in the following section, three energy flux values will be presented: F_1, F_2 and the energy flux residual, δ, defined as the time-averaged flux through the domain boundary. For an exact solution, δ would be zero. Its value is therefore an indication of solution accuracy.

4. Solutions for internal wave generation

The solution procedure developed in Section 3 will be used in this section to examine the generation of internal waves over shelf-type topography. For ease of interpretation, attention will be limited to linear slopes over which α, defined by (2.17), is constant. Solutions will be presented for a fixed bottom topography, as shown in Figure 3, representing in idealized coastal configuration. The shelf is 50 km wide and 200 m deep. The gradient of the slope is .01 and the ocean at the foot of the slope is 1000 m deep. The wave frequency ω is set to 10^{-4} s^{-1}, f is set to zero, and the surface tidal amplitude, ζ_0, is assumed to be 1 m. We shall examine the nature of the internal wave solutions for buoyancy frequencies of the order of 10^{-2} s^{-1}, with particular emphasis upon the difference in behavior between subcritical and supercritical situations.

With the given parameter values,

$$N = 10^{-2}\alpha, \tag{4.1}$$

where α is dimensionless and N has the units of s^{-1}. The examples to be presented will be classified in terms of the value of α but may also be described, using (4.1), according to the value of N.

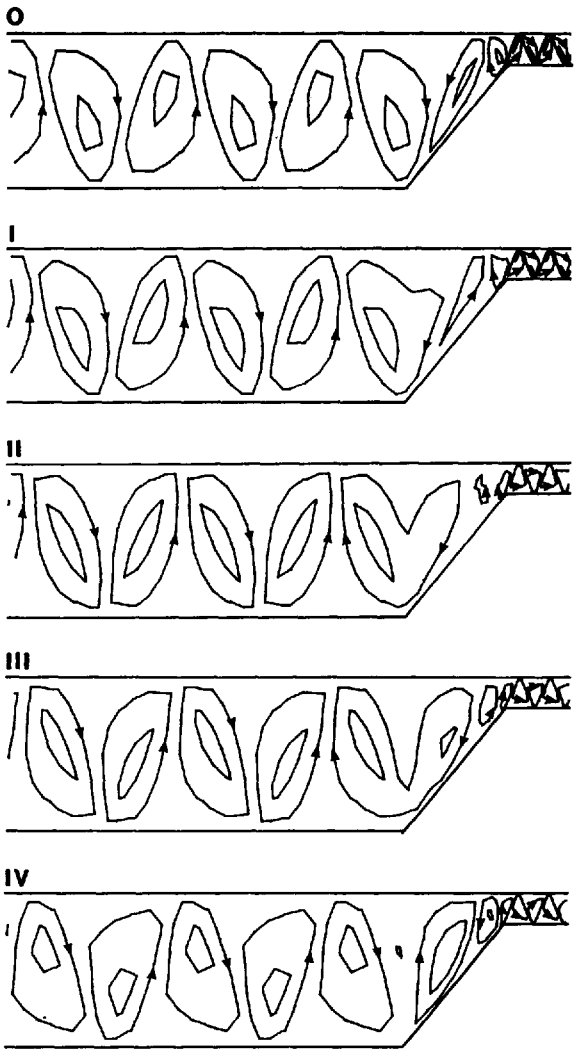

Figure 4. Generated baroclinic wave for $\alpha = 0.6$, showing streamlines over a half-period at intervals of a sixteenth-period. The Roman numerals indicate the number of sixteenth-periods past high tide. The streamline interval is 0.5 $m^2 s^{-1}$; arrowheads indicate the circulation direction.

Solutions will be presented as streamline plots. This representation allows for easy visualization of the two-dimensional structure of the waves.

It is important to note that the barotropic and baroclinic solutions do not have a separate identity over the variable topography. The barotropic solution (2.23) does not satisfy the governing equation (2.8) when N is nonzero. However, the barotropic solution for $x < x_1$ and $x > x_2$, together with the surface displacement and depth-averaged horizontal velocity component for all x are independent of the

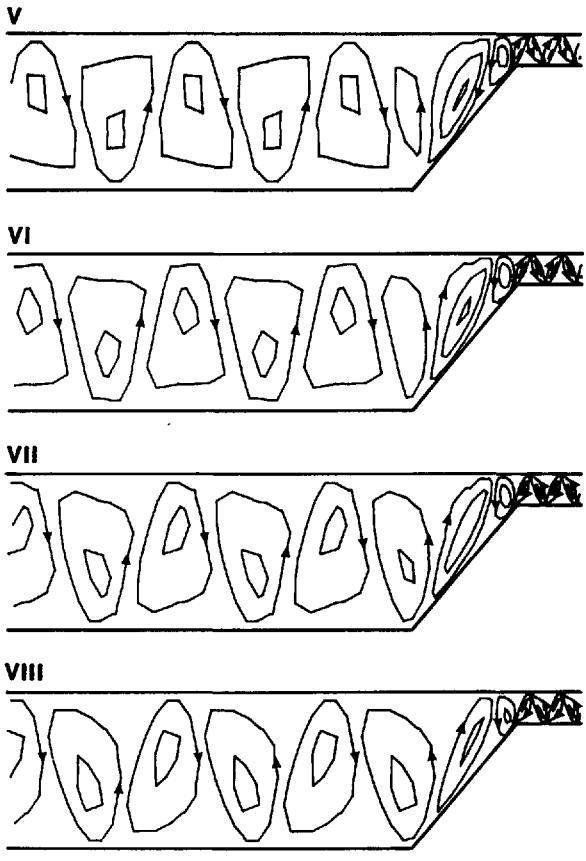

Figure 4. (Continued)

stratification. Thus, it is common practice (e.g. Baines, 1973), when N is nonzero, to regard (2.23) as 'the barotropic solution', and the difference between the total stream function and (2.23) as 'the baroclinic solution'.

Figures 4 and 5 show the baroclinic solutions, calculated using $K = M = 16$, for α equal to 0.6 and 1.4 respectively, corresponding to the grid geometries in Figure 3. The solutions are plotted over a half-wave period at successive instants separated by one-sixteenth of a period. In the second half-period, the motion is the same as in the first, but with the sign of the streamlines changed. Thus Figures 4 and 5 allow the wave motion to be followed over a full wave period.

In each figure, the phase propagation away from the slope, in the same direction as the energy propagation, is apparent. For the subcritical case (Fig. 4), there appears to be approximately equal energy propagating into the deep ocean and onto the shelf, with somewhat more energetic motion over the slope. For the supercritical case (Fig. 5) there is energetic motion over the slope and in the deep ocean with relatively little

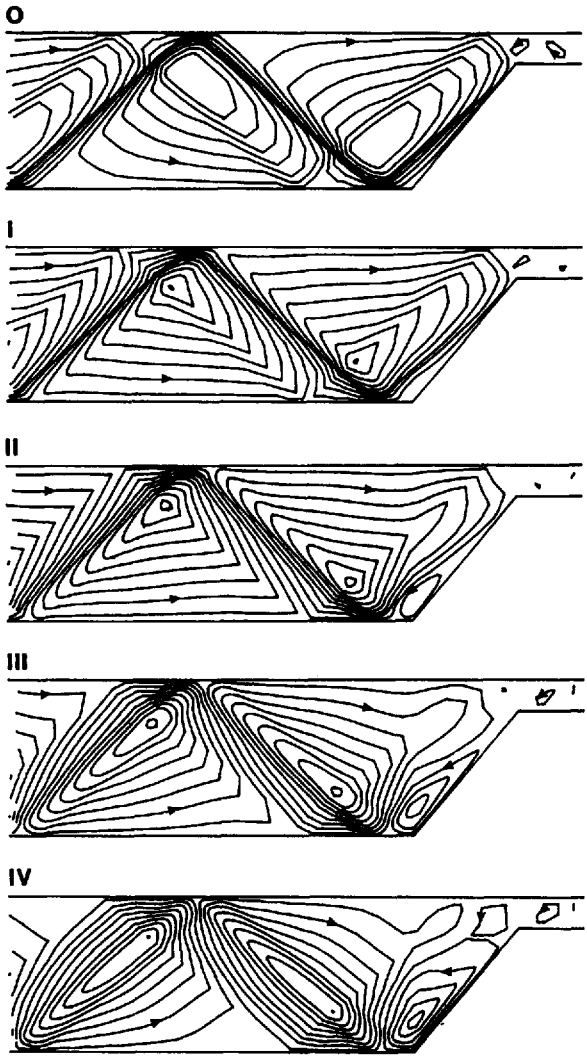

Figure 5. Generated baroclinic wave for $\alpha = 1.4$. Details are as for Figure 4.

motion over the shelf. (The shelf motion is not well resolved by the contouring in Figure 5.) There is a relatively higher energy beam, extending between parallel characteristics, from the slope region into the deep ocean for the supercritical case, and onto the shelf for the subcritical case. The highest velocities occur within these beams.

An interesting feature of Figures 4 and 5 is the manner in which the circulation cells originate over the slope discontinuities. For example, in diagram iv of Figure 4, a small cell is beginning to grow directly above the foot of the slope. This cell grows in time, and in diagrams i to iii it separates, one lobe propagating into the deep ocean, the other propagating upslope and, eventually, onto the shelf.

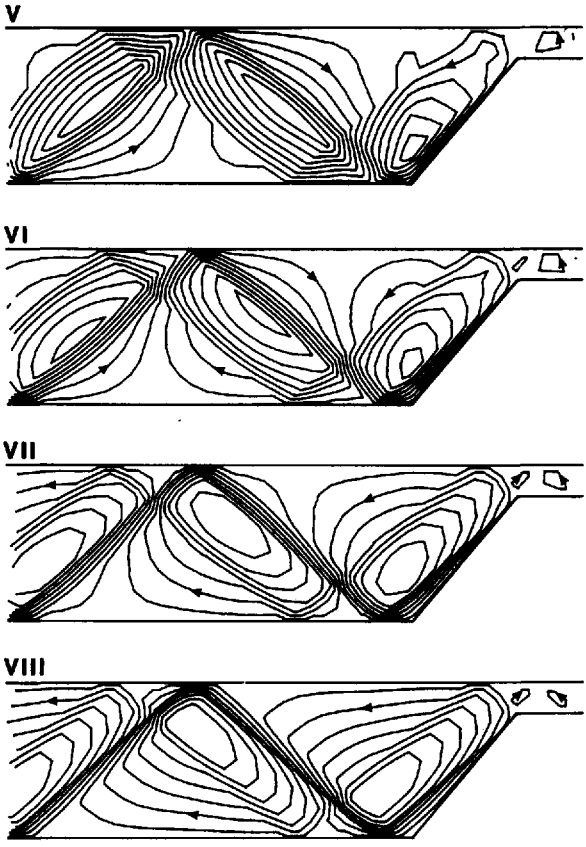

Figure 5. (Continued)

Streamlines for α values of 0.9 and 1.1, close to, but on either side of, critical, are shown in Figures 6 and 7. The streamlines exhibit the same large-scale features as those for α equal to 0.6 and 1.4. As is to be expected, there is a narrow, high-energy beam directed upslope onto the shelf in Figure 6, and downslope into the deep ocean in Figure 7. These features are more intense than those in Figures 4 and 5. It should be noted that the large-scale features over the slope and in the deep ocean show marked similarity in the sub- and super-critical solutions of Figures 6 and 7.

Table 1 lists the values of F_1, F_2 and δ for values of α ranging from 0.2 to 2 in steps of 0.2, calculated using both 8 and 16 modes at each of $x = 0$ and $x = L$. Doubling the number of modes results in an improvement in the accuracy of the solution. The error is reduced by an order of magnitude for subcritical α, but at supercritical values decreases from an order of magnitude improvement at $\alpha = 1.2$ to no improvement at $\alpha = 1.8$. Over the α-range listed in Table 1, the relative error, δ/F_1, ranges from better than .01 to .05.

Table 1 reveals major differences between the baroclinic energy fluxes for subcriti-

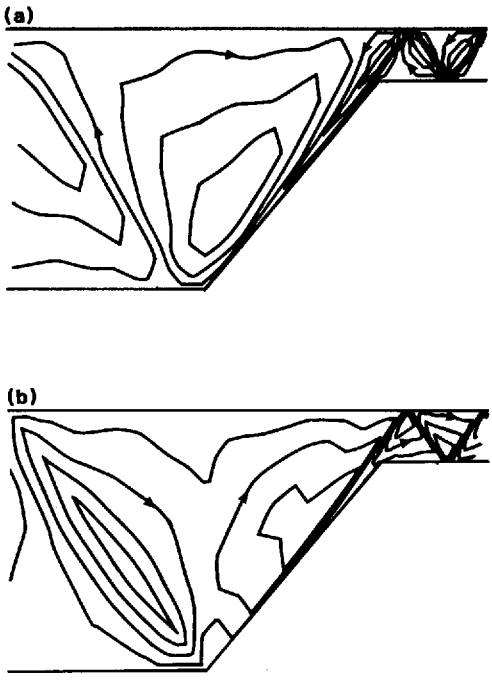

Figure 6. Generated baroclinic motion at the near-critical $\alpha = 0.9$, (a) in-phase and (b) out-of-phase with the surface tide. The streamline interval is 0.5 $m^2 s^{-1}$ and the arrowheads indicate the circulation direction.

cal and supercritical α. For subcritical α, offshore energy fluxes (F_1) and the onshore flux (F_2) are approximately equal. In addition, increases in α lead to dramatic increases in the energy flux. Increments of 0.2 in α result in increases of up to an order of magnitude in the energy flux.

For supercritical α, the energy flux onto the shelf (F_2) is of the same magnitude as the error of the calculations, being of the order of 2% of the flux directed offshore. The offshore energy flux is apparently linearly dependent on the buoyancy frequency. Increments of 0.2 in α lead to constant increments of 40 Wm^{-1} in the energy flux.

The variation of the energy flux with α will be examined in more detail in the following section.

5. Discussion

Broad features of the streamline distributions in solutions such as those of Figures 4 to 5 can be predicted from the characteristic distributions in Figure 3. In this section, it will be shown that the magnitude of the stream function can be predicted by assessment of the relative scales of the barotropic forcing and the baroclinic response.

If the total stream function, ψ, is expressed as the sum of a baroclinic component, ψ',

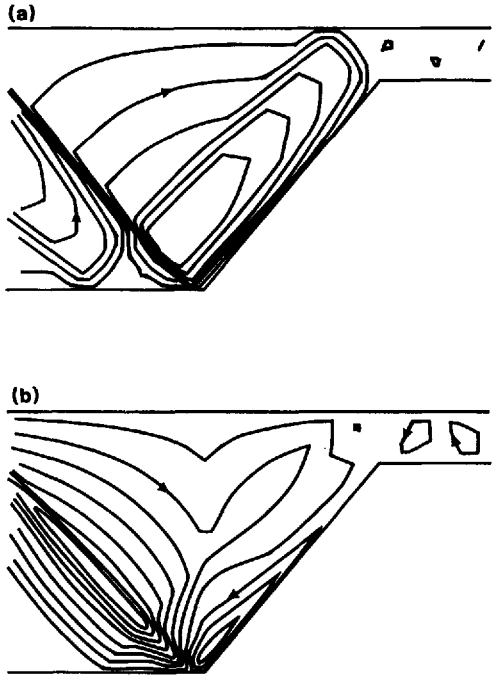

Figure 7. Streamline solution at the near-critical $\alpha = 1.1$. Details are as for Figure 6.

and the barotropic forcing defined by (2.23), (2.8) can be rewritten as

$$\psi'_{zz} - \frac{1}{c^2}\psi'_{xx} = i\frac{\omega}{c^2}\zeta_0\left(\frac{z-h}{H-h}(x-L)\right)_{xx} \tag{5.1}$$

By (2.24), we may estimate the modal coefficient a_1 by

$$a_1 \sim \tfrac{1}{2}\psi', \tag{5.2}$$

and, by (3.10), the energy propagating toward the deep ocean is estimated by

$$F_1 \sim \rho_0 N \frac{(\omega^2 - f^2)^{1/2}}{\omega}\pi a_1^2. \tag{5.3}$$

The barotropic forcing, defined by the right-hand side of (5.1), occurs over the topographic depth and length scales, Z and X say, which are in the ratio h_x. The depth to length scale ratio of the baroclinic response, defined by the left-hand side of (5.1), is c. The depth scale of the baroclinic response is again the depth scale Z, which is a physical restriction on the motion. The depth and length scales of the baroclinic motion are then Z and $(1/c)Z$. For the linear slope, when the flow is subcritical, $c > h_x$ and the response length scale is less than the topographic length scale. In the supercritical case, $c < h_x$ and the response length scale is greater than the topographic scale.

Table 1. Baroclinic energy flux toward the deep ocean (F_1) and onto the shelf (F_2), and energy flux residuals (δ) in Wm^{-1}, for bottom to characteristic slope ratio α ranging from 0.2 to 2.0. Results are shown for calculations using 8 and 16 modes.

	16 modes			8 modes		
α	F_1	F_2	δ	F_1	F_2	δ
0.2				.071	.065	.0021
0.4	.74	.70	.034	.92	.73	.10
0.6	4.5	3.1	.0071	5.1	3.5	.67
0.8	12	12	−.085	11	12	−.031
1.2	150	6.2	6.8	180	13	49
1.4	190	6.5	9.3	190	18	20
1.6	230	6.5	4.9	230	11	12
1.8	270	7.2	3.7	260	11	−3.4
2.0	300	11	5.5	280	12	6.2

The relationship between the length scales can be clearly seen in the subcritical and supercritical solutions of Figures 4 and 5. In the subcritical case, baroclinic circulation cells over the slope are narrower than the slope region. In the supercritical case, they extend well beyond the slope into the deep ocean region.

The consequence of these relative length scales is that, in assessing the forced response, the appropriate length scale, over which the effective forcing occurs, is $(1/c)Z$ for subcritical slopes and X for supercritical slopes.

If, from (5.1), we define

$$\beta = \omega\zeta_0\left(\frac{z - h}{H - h}(x - L)\right)_{xx}, \tag{5.4}$$

then the magnitude of the baroclinic stream function may be estimated by

$$\psi'_{xx} \sim \beta. \tag{5.5}$$

For the subcritical case, $x \sim (1/c)Z$, so that

$$\psi' \sim c_1\alpha^2 \tag{5.6}$$

and

$$F_1 \sim c_2\alpha^5, \tag{5.7}$$

where

$$c_1 = \beta X^2 \tag{5.8}$$

and

$$c_2 = \tfrac{1}{4}\rho_0\pi\beta^2X^5(\omega^2 - f^2)\,(\omega Z)^{-1}. \tag{5.9}$$

Table 2. Comparison between F_1 (in Wm^{-1}) from full model calculation and that estimated by order-of-magnitude formulae (5.7) and (5.11)

α	F_1 from Table 1	F_1 by formulae
0.2	.071	.04
0.4	.74	1.3
0.6	4.5	10
0.8	12	40
1.2	150	150
1.4	190	175
1.6	230	200
1.8	270	226
2.0	300	251

For the supercritical case, $x \sim X$, so that

$$\psi' \sim c_1, \tag{5.10}$$

and

$$F_1 \sim c_2 \alpha. \tag{5.11}$$

Thus, simple scaling analysis predicts that the energy flux varies as α^5 for subcritical buoyancy frequencies, but is linearly dependent on α for supercritical frequencies.

Substitution of appropriate parameter values provides a quantitative test of the arguments leading to (5.7) and (5.11). A comparison between F_1 predicted by (5.7) and (5.11) and that in Table 1 is listed in Table 2 and plotted in Figure 8. The

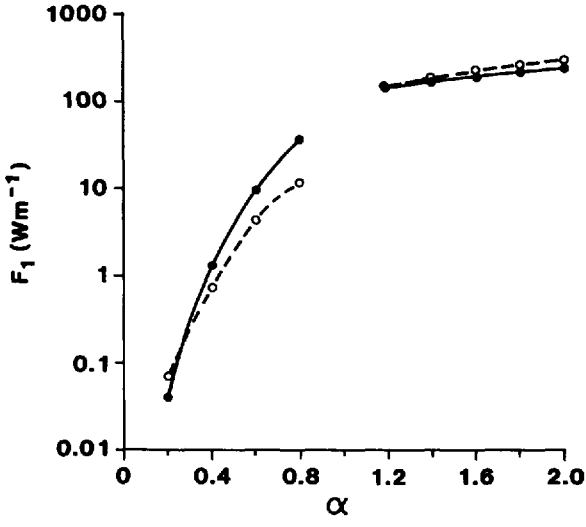

Figure 8. Log-linear plot of energy flux F_1 against α for full model calculation (dashed line) and order-of-magnitude formulae (continuous line).

parameter values used in the calculations were: $\omega = 10^{-4}$ s^{-1}, $f = 0$, $\zeta_0 = 1$ m, $(z - h)/(H - h) \simeq 0.5, X = 8 \times 10^4$ m, $Z = 800$ m, $x - L \simeq X, \partial^2/\partial x^2 \sim 1/X^2$ and $\rho_0 = 10^3$ kg m^{-3}.

Given the high powers involved in (5.7) and (5.11), and the arbitrariness in choice of scales, the agreement in Table 2 and Figure 8 is surprisingly good. Manipulation of the scales can lead to better agreement. For instance, use of the average depth over the slope, 600 m, as the estimator for Z in (5.7) gives values of F_1 of .01, .4, 3 and 13 Wm^{-1}, for subcritical α corresponding to those in Table 2.

The order of magnitude relationship (5.6) states simply that, for subcritical bottom slopes, the amplitude of the internal wave motion varies proportionally with the background vertical density gradient. In simple terms, the greater the buoyancy frequency, the greater the horizontal density gradient set up by the motion due to the surface tide, and hence the stronger the baroclinic response.

For supercritical slopes, an increase in N not only increases the horizontal density gradient caused by the surface tides, but also increases the distance over which the response must occur to beyond the horizontal extent of the topography. The effect of the forcing, which occurs over the topographic length scale, must be 'spread' over the baroclinic length scale to maintain the motion. These two effects cancel one another and the order of magnitude result (5.10) indicates that, for supercritical slopes, the amplitude of the stream function is independent of N. This means that the vertical velocities and displacements may actually decrease with increasing N, while the order of the horizontal velocity components will not change.

It is apparent from the form of (5.7) and (5.11) that the offshore energy flux F_1 is predicted to be a continuous function of α at the critical slope. This continuity may be also inferred from the similarity of the solutions in the deep ocean in Figures 6 and 7. By contrast, the onshore energy flux F_2 will decrease dramatically with the transition from subcritical to supercritical conditions.

The full time-development of the solutions in Figures 6 and 7 may be inferred from Figures 4 and 5 respectively. In each of the in-phase plots of Figures 6 and 7 there is a triangular cell, centered over the foot of the slope, whose shape and size is determined by the domain boundaries and the characteristics from the foot of the slope. One quarter of a period later, the cell is splitting. In each case, the lobe over the slope propagates similarly to a free wave, reflecting upslope from the subcritical boundary, and downslope from the supercritical.

From each point on the subcritical slope, the ξ-characteristic is directed offshore and the η-characteristic onshore. There is approximately equal energy propagation offshore and onshore, so that (5.6) serves as an estimator for ψ' over the shelf, and (5.7) may also be used to estimate F_2.

For the supercritical case, however, most of the baroclinic energy propagating onto the shelf appears likely to be generated upslope of the ξ-characteristic from the shelf break, that is, in the triangular region between this characteristic and the vertical line

through the shelf break. This hypothesis can again be tested using the order of magnitude relationships. In this region, since the baroclinic length scale is less than the topographic length scale (5.6) and (5.7) again apply, but with $Z = 200$ m, and $x = 2 \times 10^4$ m. By (5.7), F_2 is then estimated as 5.1 and 16 Wm^{-1} at $\alpha = 1.6$ and 2.0 respectively. These values are consistent with those of 6.5 and 11 Wm^{-1} in Table 1.

Using (5.7) with $\alpha = 1$ and the appropriate scales, F_2 is estimated to drop from 125 to 0.49 Wm^{-1} with the transition from α subcritical to α supercritical. With α supercritical, F_2 is then expected to increase again as α^5.

There are many subtleties which are not described by the scaling analysis, and care must be taken with its application. One such subtlety is the following. At $\alpha = 0.67$, the ξ-characteristic through the shelf break reflects from the surface as an η-characteristic which passes exactly through the foot of the slope. For this α, most of the baroclinic energy is trapped over the slope, and very little propagates into the deep ocean or onto the shelf. This phenomenon was also noted by Baines (1973) and Sandstrom (1976). In this case, although (5.6) still remains a good estimation of the magnitude of ψ over the slope, (5.7) dramatically overpredicts the energy flux F_1.

It is stressed that the reasoning of the present section has been applied only to a linear slope. For other topographies, the relationship between forcing (topographic) length-scales and response (baroclinic) length-scales will not be so simple, but extension of the concepts developed in the section should not prove difficult.

6. Concluding comments

The major advantage of the solution technique described in the present paper is its simplicity. The technique is strictly algebraic in its implementation and, in providing a solution to the stream function equation (2.8), requires as its only approximation the truncation of the modal series. By appropriate choice of the number of modes, it is possible to resolve the solution over arbitrarily complex topography.

As demonstrated in Section 4, the technique may be used to examine solutions at topographic slopes close to critical. These solutions indicate the mathematical behavior as the critical slope is approached, providing information on the location of regions of high shear and energy flux. In reality, these regions will be highly frictional and nonlinear. Detailed description of the dynamics in such regions will require specialist models incorporating these additional physical influences (e.g. Gordon, 1980).

For general oceanographic application, the most severe limitation of the solution technique is the restriction to a buoyancy frequency independent of depth. This may be a good approximation for water near the shelf break, particularly in thermally stratified tropical waters (e.g. Holloway, 1984). However, it will never be a good approximation in the deep ocean.

With a z-dependent density gradient, the stream function equation (2.8) remains unchanged. The characteristics are, however, no longer straight, and characteristic

functions ϕ and γ can in general no longer be defined. In this case, solution of the equation requires resort to numerical techniques. One approach, described by Chuang and Wang (1981), is to use standard finite-difference stepping procedures. This approach has the disadvantage that it takes no account of the properties of the characteristics, nor of the relationship between the characteristic slope and the bottom slope. Alternatively, it is possible to modify the technique described in the present paper.

Definition of the functions ϕ and γ effectively represents analytic integration of the governing equation (2.8) along the characteristics. With N variable, the integration may no longer be performed analytically, but may be approximated numerically. The characteristic traces (e.g. Fig. 3) may then be regarded as a grid upon which two-dimensional numerical integration may be undertaken. With this approach, the modal representations of the solution at each end of the domain may be related, again leading to a set of linear algebraic equations in the modal coefficients.

Numerical extension of the solution technique is described in detail in Craig (1986). Preliminary results indicate that the dynamics are qualitatively similar in the presence of variable N. Details of the solutions vary, however, so that, for comparison with data, the model must include an accurate representation of the vertical density profile. The order of magnitude formulae introduced in Section 5 still appear to result, with correct definition of the x and z scales, in good estimates of the baroclinic amplitude.

Numerical solution of a hyperbolic equation in a partially bounded domain is not a trivial problem. There is considerable attraction in the use of a simple analytic technique, such as the one described in Section 3, in studies of internal tidal generation and propagation. This form of study can be made site-specific by use of the relevant topographic profile, leading to a qualitative understanding of the local internal tidal dynamics, and their response to changing density gradients.

Acknowledgments. I wish to thank Dr Peter Holloway for his support throughout this study, and Dr John Church for his helpful comments on the manuscript. Most of the work described in this paper was undertaken for a doctoral dissertation at the University of Western Australia, supervised by Professor J. Imberger and financially assisted by a University of Western Australia Postgraduate Studentship.

REFERENCES

Baines, P. G. 1973. The generation of internal waves by flat-bump topography. Deep-Sea Res., *20,* 179–205.

—— 1974. The generation of internal tides over steep continental slopes. Philos. Trans. R. Soc. Lond., *A277,* 27–58.

——1982. On internal tide generation models. Deep-Sea Res., *29,* 307–338.

Battisti, D. S. and A. J. Clarke. 1982. A simple method for estimating barotropic tidal currents on continental margins with specific application to the M_2 tide off the Atlantic and Pacific coasts of the United States. J. Phys. Oceanogr., *12,* 8–16.

Chuang, W-S and D-P Wang. 1981. Effects of a density front on the generation and propagation of internal tides. J. Phys. Oceanogr., *11,* 1357-1374.

Craig, P. D. 1986. Numerical modelling of internal tides, *in* Numerical Modelling—Applications to Marine Systems, B. J. Noye, ed., Elsevier, Amsterdam 107–122.

Gill, A. E. 1982. Atmosphere-Ocean Dynamics, Academic Press, NY, 662 pp.

Gordon, R. L. 1980. Boundary layer under near-inertial internal waves over a critically sloping bottom. J. Phys. Oceanogr., *10,* 1032–1038.

Holloway, P. E. 1984. On the semidiurnal internal tide at a shelf-break region on the Australian North West Shelf. J. Phys. Oceanogr., *14,* 1787–1799.

LeBlond, P. H. and L. A. Mysak. 1978. Waves in the Ocean, Elsevier, Amsterdam, 602 pp.

Prinsenberg, S. J. and M. Rattray, Jr. 1975. Effects of continental slope and variable Brunt-Vaisala frequency on the coastal generation of internal tides. Deep-Sea Res. *22,* 251–263.

Prinsenberg, S. J., W. L. Wilmot and M. Rattray, Jr. 1974. Generation and dissipation of coastal internal tides. Deep-Sea Res., *21,* 263–281.

Rattray, M. Jr. 1960. On the coastal generation of internal tides. Tellus, *22,* 54–62.

Rattray, M. Jr., J. G. Dworski and P. E. Kovala. 1969. Generation of long internal waves at the continental slope. Deep-Sea Res., *16* (Suppl.) 179–195.

Sandstrom, H. 1976. On topographic generation and coupling of internal waves. Geophys. Fluid Dyn., *7,* 231–270.

Wunsch, C. 1968. On the propagation of internal waves up a slope. Deep-Sea Res., *15,* 251–258.

—— Progressive internal waves on slopes. J. Fluid Mech., *35,* 131–141.

Received: *30 June, 1986;* revised: *25 November, 1986.*